Electrochemical behaviour of Lanthanum fluoride and Praseodymium fluoride on inert and reactive electrodes in molten LiF-CaF2

Laurent Massot, Mathieu Gibilaro, J. Nicaise, Pierre Chamelot

Electrochemical behaviour of Lanthanum fluoride and Praseodymium fluoride on inert and reactive electrodes in molten LiF-CaF_2

L. Massot*, M. Gibilaro, J. Nicaise, P. Chamelot

Laboratoire de Génie Chimique; Université de Toulouse; CNRS; INPT; UPS;

Toulouse, France

* Corresponding author

massot@chimie.ups-tlse.fr

tel: +33 5 61 55 81 94

fax: +33 5 61 55 61 39

Abstract

Electrochemical behaviour of La(III)/La and Pr(III)/Pr systems has been studied in LiF-CaF_2 media (79.5%-20.5%) on inert and reactive electrodes in the 820-930°C temperature range using cyclic voltammetry, square wave voltammetry and open-circuit potentiometry. Experimental results show that La(III) and Pr(III) are reduced into metal in a one-step and diffusion controlled process, exchanging 3 electrons, at 0.08 and 0.15 V vs. LiF/Li respectively. Physico-chemical and thermodynamic data such as diffusion coefficients, standard potential, activity coefficients, have been determined. Effect of oxide additions have been investigated and leads to precipitation of LaOF and PrOF species. Alloys formation by reactive electrodeposition on Ni, Cu and Fe electrodes has also been evidenced and their Gibbs energies determined.

Keywords

electrochemistry, Lanthanum, Praseodymium, molten fluoride, cyclic voltammetry

1/ Introduction

Rare Earth elements (REEs) are increasingly used or investigated for many industrial applications, such as spent nuclear fuel reprocessing [1-4], renewable energy technologies (permanent magnets [5] and Ni-MH batteries [6, 7], optical and optoelectronic devices for solid-state lasers [8]). They are also used in metallurgy industry to improve corrosion resistance or ductility of steel in oxidizing media at high temperature [9]. To prevent lack of supply from REEs minerals, the recovery of REEs from their secondary sources are under investigation [10, 11] and is of significantly importance for sustainable rare-earth industry. For example, recycling End-of-Life Ni-MH batteries is hardly developed, while 6 to 10 wt.% of those batteries are constituted of REEs, depending of the battery type (button cell,

cylindrical cell, …) [7]. Initially, batteries anodes are constituted of lanthanum-nickel alloy ($LaNi_5$) but lanthanum is usually substituted by mischmétal (La-Ce-Pr-Nd alloy) for economic considerations. One way to separate and recover REEs is molten salts electrolysis using molten halides (chlorides, fluorides) as solvent. In these media, electrochemical behaviour of REEs precursor with and without oxides is needed for electrodeposition processes as well as physico-chemical and thermodynamic data.

From all REEs, this work concerns two lanthanides: Lanthanum and Praseodymium. Several electrochemical studies of La(III) and Pr(III) behaviour have been performed into molten chloride media [12-18]. All these works evidenced that the electrochemical reduction pathway of both La(III) and Pr(III) occurred in a one-step process exchanging three electrons and limited by the diffusion of $LnCl_3$ in the bath:

$$LnCl_3 + 3\ e^- = Ln + 3\ Cl^- \quad (Ln = La, Pr) \qquad (1)$$

The influence of oxide additions on La(III) and Pr(III) stability was also examined and the the same results were obtained for both elements, leading to the precipitation of LnOCl:

$$LnCl_3 + O^{2-} = LnOCl + 2\ Cl^- \qquad (Ln = La, Pr) \qquad (2)$$

Concerning molten fluoride media, many La(III) and Pr(III) thermodynamic properties are missing. R. Chesser *et al.* [1] and Y. Wang *et al.* [2] studied La(III) electrochemical behaviour into LiF-NaF-KF and LiF-(NaF/KF) media respectively and evidence a one-step reduction process exchanging 3 electrons:

$$LaF_3 + 3\ e^- = La + 3\ F^- \qquad (3)$$

The authors proposed relationships between diffusion coefficient and temperature on one hand and apparent standard potential and temperature on the other hand. Yasuda *et al.* investigated Pr(III) electrochemical reduction and evidenced a similar behaviour [19]:

$$PrF_3 + 3\ e^- = Pr + 3\ F^- \qquad (4)$$

This work presents a complete electrochemical investigation of both La(III) and Pr(III) on inert (Mo) and reactive (Ni, Cu, Fe) electrodes into LiF-CaF_2 medium with and without oxides to acquire data such as diffusion coefficients, standard potential, activity coefficients and alloys formation Gibbs energies of Ni/Cu/Fe - La/Pr alloys in a wide range of temperature.

2/ Experimental

The cell consisted of a vitreous carbon crucible placed in a cylindrical vessel made of refractory steel closed by a lid cooled by circulating water. The inner part of the cell was protected against fluoride vapours by a graphite liner. Experiments were performed under an inert argon atmosphere (99.999%). The cell was heated using a programmable furnace and the temperatures were measured using a chromel-alumel thermocouple. The electrolytic bath consisted of a eutectic LiF-CaF_2 (Merck 99.99%) mixture (79.5/20.5 molar ratio), initially dehydrated by heating under vacuum (10^{-5} bar) to its melting point.

Lanthanum and Praseodymium ions were introduced in the form of LaF_3 and PrF_3 powder (VWR 99.99%) respectively and oxide ions in the form of Li_2O powder (Cerac 99.9%).

Molybdenum, nickel, copper and iron wires (Goodfellow 99.99%, 1mm diameter) were used as working electrodes. The auxiliary electrode was a vitreous carbon rod (3 mm diameter) with a large surface area (5 cm^2).

All the potentials were referred to the equilibrium potential of LiF/Li system, measured on the cyclic voltammograms plotted using an inert molybdenum working electrode.

The electrochemical study and the electrolyses were performed with an Autolab PGSTAT 302N potentiostat / galvanostat controlled with NOVA 2.10 software. Cyclic voltammetry and

open-circuit chronopotentiometry were the electrochemical techniques used for the investigation of the reduction pathway and data acquisition.

3/ Results and discussion

3-1/ Electrochemical behaviour on inert electrode

The electrochemical behaviour of La(III) and Pr(III) was first investigated on inert (Mo) electrode in the LiF-CaF_2-LaF_3 and LiF-CaF_2-PrF_3 systems at 850°C by cyclic voltammetry.

3-1-1/ Cyclic voltammetry:

Figure 1 presents typical cyclic voltammograms plotted on Mo electrode at 100 $mV.s^{-1}$ and 850°C for LiF-CaF_2-LaF_3 (0.138 $mol.kg^{-1}$) (grey line) and LiF-CaF_2-PrF_3 (0.136 $mol.kg^{-1}$) (black line) systems respectively. Both voltammograms exhibit a single cathodic peak at 0.07 V vs. LiF/Li for La(III) and 0.15 V vs. LiF/Li for Pr(III). Each cathodic peak is correlated to one reoxidation peak with a stripping shape characteristic of solid phase dissolution.
As presented in the Fig. 1 inset, the quasi-reversibility of both systems, characterized by La(III) and Pr(III) reduction peak potentials independent of the scan rate, is verified.
The influence of the scan rate on La(III) and Pr(III) reduction peak current densities is also presented in the Fig. 1 inset, in order to verify the Berzins Delahaye relationship, valid for a reversible soluble/insoluble system and a diffusion-controlled reaction [20]:

$$I_p = -0.61nFSc_0\left(\frac{nF}{RT}\right)^{1/2} D^{1/2} v^{1/2} \qquad (5)$$

where n is the number of exchanged electrons, F the Faraday constant (96500 C), S the electrode surface area in cm^2, D the diffusion coefficient in $cm^2\ s^{-1}$, c_0 the solute concentration in mol cm^{-3}, T the absolute temperature in K and v the potential scan rate in V s^{-1}.

The slope of these linear equations at 840°C, proving that reactions are controlled by Ln(III) diffusion into the solution, are:

- For La(III) reduction: $\frac{\mathbf{i_p}}{\mathbf{v^{1/2}}} = \mathbf{-0.639\ A\ s^{1/2}V^{-1/2}cm^{-2}}$ (6)

- For Pr(III) reduction: $\frac{\mathbf{i_p}}{\mathbf{v^{1/2}}} = \mathbf{-0.689\ A\ s^{1/2}V^{-1/2}cm^{-2}}$ (7)

The variation of the cathodic peak current density as function of molality is presented in Figure 2, for La(III)/La (grey) and Pr(III)/Pr (black) systems. This figure shows a linear dependency for both elements, confirming that this peak is attributed to the reduction of Ln(III) into Ln (cf. eqs 3 and 4). The relationships between the intensity of the reduction peak and the molality is given at 840 °C:

j_p = -1.47 [La(III)] (8)

j_p = -1.62 [Pr(III)] (9)

where j_p the peak current density, [La(III)] and [Pr(III)] the lanthanide molality (mol kg^{-1}).

3-1-2/ Diffusion coefficient determination

As shown in eq. (5), diffusion coefficient can be determined from Berzins-Delahay equation using the linearity between the peak current density and the square root of scanning rate. For instance in Figure 1 at 850°C, the obtained values of diffusion coefficient are:

$D_{La(III)} = 5.49x10^{-6}\ cm^2s^{-1}$ (10)

$D_{Pr(III)} = 6.53x10^{-6}\ cm^2s^{-1}$ (11)

Experiments were performed at several temperatures (from 840 to 930 °C) and the obtained values, plotted fig. 3, show that the variation of diffusion coefficient with the temperature obeys Arrhenius' like law expressed as:

$$\ln\left(D_{La(III)}\right) = -7.728 - \frac{4871.1}{T_{(K)}} \quad (12)$$

$$\ln\left(D_{Pr(III)}\right) = -7.206 - \frac{5270.3}{T_{(K)}} \quad (13)$$

3-1-3/ Ln(III)/Ln standard potential determination

According to the Nernst Law, the equilibrium potential of Ln(III)/Ln system, $E_{Ln(III)/Ln}$, is expressed as follows:

$$E_{Ln(III)/Ln} = E^{o}_{Ln(III)/Ln} + \frac{RT}{3F}\ln\left(\gamma_{Ln(III)}\right) + \frac{RT}{3F}\ln([Ln(III)]) \quad (14)$$

where $\gamma_{Ln(III)}$ and [Ln(III)] are the activity coefficient and the molality in mol kg^{-1} of dissolved Ln(III) respectively (Ln = La, Pr).

$E_{Ln(III)/Ln}$ can be measured from the cyclic voltammogramm of LiF-CaF_2-LnF_3 systems, but it must be previously converted into a reference potential scale using the F_2/F^- system, using the equilibrium potential of LiF/Li versus F_2/F^-, as detailed in ref [21], where $E_{LiF/Li\ vs.\ F_2/F^-}$ = -5.30 V.

According to (14):

$$E_{Ln(III)/Ln} - \frac{RT}{3F}\ln([Ln(III)]) = E^{o}_{Ln(III)/Ln} + \frac{RT}{3F}\ln\left(\gamma_{Ln(III)}\right) \quad (15)$$

So at a given temperature, when [Ln(III)] tends towards 0, indeed at infinite dilution $\gamma = 1$, the extrapolation of the experimental value of $E_{Ln(III)/Ln} - \frac{RT}{3F}ln([Ln(III)])$ versus [Ln(III)] allows the determination of the Ln(III)/Ln standard potential.

These relationships were plotted for La(III)/La and Pr(III)/Pr systems on Figure 4, and the obtained values are: $E^{o}_{La(III)/La} = -5.03$ V vs. F_2/F^- and $E^{o}_{Pr(III)/Pr} = -4.95$ V vs. F_2/F^-

3-1-4/ Influence of Li_2O additions

The influence of oxide additions on the stability of La(III) and Pr(III) ions was investigated by plotting cyclic voltammograms of LiF-CaF_2-LnF_3 systems, on Mo electrode at 100 $mV.s^{-1}$ and 840°C after successive Li_2O additions. The measure of cathodic peak current density for both La(III) and Pr(III) reduction can be converted into normalised quantity (mol) of species remained into the bath, using eqs. (8) and (9): $\frac{n_{Ln(III)}}{n^{o}_{Ln(III)}}$ with Ln = La, Pr and $n°_{Ln(III)}$ is the quantity of Ln(III) initially present into the solution.

These normalised Ln(III) quantities $\frac{n_{Ln(III)}}{n^{o}_{Ln(III)}}$ were plotted versus the normalised oxide ions content $\frac{n_{Li_2O}}{n^{o}_{Ln(III)}}$, where n_{Li_2O} is the added quantity of O^{2-} in mol.

The results, presented in Figure, exhibit for both elements a linear relationship with a slope of -1 between the normalised quantity of oxide added and the normalised Ln(III) quantity remaining in the solution. After addition of a normalized oxide content more than 1, no more electrochemical signal related to the Ln(III)/Ln systems can be observed. This behaviour is an evidence of a solid formation, or non-electroactive compounds.

Regarding the thermodynamic data on La and Pr species, the following Ln(III) precipitation reaction can be assumed:

$$LnF_3 + O^{2-} \leftrightarrow LnOF + 2F^- \qquad (Ln = La, Pr) \qquad (16)$$

The experimental results are in agreement with the stoichiometry of precipitation reaction observed into molten fluorides for other REEs fluorides already evidenced in our laboratory [22].

3-2/ Electrochemical behaviour and alloys formation on reactive electrode

Study of La and Pr alloys formation was performed on three metallic substrates: Ni, Cu and Fe. Analysis of the phase diagrams from ref [23] shows the existence of the following intermetallic compounds for each system:

- La-Ni system: $NiLa_3$, Ni_3La_2, Ni_2La, Ni_3La, Ni_7La_2, Ni_5La
- La-Cu system: $CuLa$, Cu_2La, Cu_5La, Cu_6La
- La-Fe system: no alloy formation
- Pr-Ni system: $NiPr_3$, Ni_3Pr_7, $NiPr$, Ni_2Pr, Ni_3Pr, Ni_7Pr_2, Ni_5Pr
- Pr-Cu system: $CuPr$, Cu_2Pr, Cu_4Pr, Cu_5Pr, Cu_6Pr
- Pr-Fe system: Fe_2Pr, $Fe_{17}Pr_2$

Alloys formation was evidenced by cyclic voltammetry and open-circuit chronopotentiometry, and characterised by SEM-EDS.

3-2-1/ Evidence of alloys formation:

Cyclic voltammetry was performed on Ni, Cu and Fe substrates at 100 $mV.s^{-1}$ and 840°C in the $LiF-CaF_2-LnF_3$ (Ln = La, Pr) (0.138 $mol.kg^{-1}$) systems. Figures 6a and 6b compare La(III) and Pr(III) reduction on reactive and on inert Mo electrode (dash line). It can be noted that for all systems, except La-Fe, the measured current densities were higher on reactive than on inert electrode. Based on the Nernst law, a lower activity of Ln in the cathodic product is expected as the reduction of Ln(III) into Ln intermetallic compound promotes the shift of the electroreduction potential towards higher values, called depolarization effect. The additional currents are attributed to alloys formation:

$$Ln(III) + 3\ e^- + x\ M = LnM_x \qquad (16)$$

(Ln = La, Pr; M = Ni, Cu, Fe).

Moreover, the La-Fe system doesn't present any alloy formation, in agreement with the La-Fe phase diagram [23].

The potential difference between reductions on inert and reactive electrodes, highlighted on the Figures 6a and 6b, represents the depolarization potential of Ln(III) electrochemical reduction and values are gathered in Table 1.

3-2-2/ Gibbs energy calculation:

Open circuit chronopotentiometry allows the identification of every compound in the Ln-M system and thus, the Gibbs energy to be calculated. The method consists in first electrodepositing a small quantity of Ln on the cathode by a short cathodic run, and then measuring the cathode open circuit potential versus time. The intermetallic diffusion of Ln and M leads to the successive formation of Ln/M compounds, with a decreasing Ln content from the substrate to the electrolyte interface [24-27].

The open-circuit chronopotentiograms plotted at 840°C on Fe, Cu and Ni substrates are shown in Figures 7, 8a, 8b, 9a and 9b respectively. These curves exhibit typical plateaus of metallic interdiffusion leading to successive intermetallic compounds at the electrode surface as expected. Each potential plateau is referred to the standard potential of the Ln, thus allowing the Ln_xM/Ln_yM_m // $LiF\text{-}CaF_2\text{-}LnF_3$/Ln emf determination, associated to the reaction:

$$Ln_xM + (y\text{-}x)\ Ln + (m\text{-}1)\ M = Ln_yM_m \qquad (17)$$

(Ln = La, Pr; M = Ni, Cu, Fe).

Measurement of these plateaus leads to the determination of alloys Gibbs energies as detailed in [27; 28]. The same experiments were carried out in the 840 – 930°C temperature range and all the values, expressed in kJ per mol of Ln, are summarized in Tables 2, 3 and 4.

4/ Conclusion

The La(III) and Pr(III) electrochemical behaviour has been investigated in the LiF-CaF_2-LaF_3 and LiF-CaF_2-PrF_3 system on inert (Mo) and reactive (Ni, Cu, Fe) electrodes. The electrochemical study evidenced an electrochemical reduction pathway similar for both La(III) and Pr(III): reduction into metal occurred in a one-step process exchanging 3 electrons and limited by the diffusion into the solution. Diffusion coefficients have also been determined on a wide temperature range (840-930°C) and data show a dependence of ln D with the inverse of the temperature, as a classical Arrhenius-type law.
La(III)/La and Pr(III)/Pr standard potentials using cyclic voltammetry. The stability of La(III) and Pr(III) species in the presence of oxide ions was also examined and the results evidenced the formation of solid LaOF and PrOF compounds. The electrochemical study on reactive electrodes show the formation of surface alloys layers Ln-M (Ln = La, Pr; M = Cu, Ni, Fe) except for Fe/La system, considered as inert electrode. Thanks to open-circuit chronopotentiometry, alloys formation Gibbs energies were determined for each compound.

References

[1] R. Chesser, S. Guo, J. Zhang, Annals of Nuclear Energy 120 (2018) 246-252.

[2] Y. Wang, J. Ge, W. Zhuo, S. Guo, J. Zhang, Electrochemistry Communications 104 (2019) 106468.

[3] Y-I. Liu, H. Ren, T-Q. Yin, D-W. Yang, Z-F Chai, W-Q. Shi, Electrochimica Acta 326 (2019) 134971.

[4] H. Tang, H. Deng, Q. Ren, D. Cai, Y. Ren, L. Shao, Y. Yan, M. Zhang, Journal of Rare Earths 34-4 (2016) 428-433.

[5] Y. Yusheng, L. Chaoqun, G. Lingyun, A, Zhuoqing, Z. Zengwu, L. Baowei, Separation and Purification Technology 233 (2020) 116030.

[6] A.M. Bernardes, D.C.R. Espinosa, J.A.S. Tenório, Journal of Power Sources, 130 (2004) 291-298.

[7] L. Grandell, A. Lehtilä, M. Kivinen, T. Koljonen, S. Kihlman, L.S. Lauri, Renewable energy, 95 (2016) 53-62.

[8] P.P Fedorov, A.A Alexandrov, Journal of Fluorine Chemistry 227 (2019) 109374.

[9] S. Wang, Q. Li, X. Ye, Q. Sun, Z. Wu, Transactions of Nonferrous Metals Society of China 23 (2013) 3104-3111.

[10] L. Omodora, S. Pitkäaho, E.M. Turpeinen, P. Saavalainen, K. Oravisjärvi, R.L. Keiski, Journal of Cleaner Production 236 (2019) 117573.

[11] N. Krishnamurthy, C.K. Gupta, Extractive metallurgy of rare earth 2nd edition, CRC Press (2016).

[12] Y.-L.Liu, G.-A.Ye, K.Liu, L.-Y.Yuan, Z.-F.Chai, W.-Q.Shi, Electrochimica Acta 168 (2015) 206-215.

[13] P.Masset, R.Konings, R.Malmbeck, J.Serp, J.-P.Glatz, Journal of Nuclear Materials 344 (2005) 173-179.

[14] Y.Castrillejo, M.R.Bermejo, A.M. Martinez, P.Diaz, Journal of Mining and Metallurgy, 39 (1-2) B (2003) 109-135.

[15] H.Tang, B. Pesic, Electrochimica Acta 199 (2014) 120-130.

[16] H.Tang, Y.-D.Yan, M.-L. Zhang, X.Li, W.Han, Y.Xue, Z.-J.Zhang, H.He, Electrochimica Acta 107 (2013) 209-215.

[17] Y.Castrillejo, M.R.Bermejo, A.M. Martinez, P.Diaz, Journal of Mining and Metallurgy, 360 (2007) 32-42.

[18] Y.Castrillejo, M.R.Bermejo, P.Diaz, A.M. Martinez, E.Barrado, Journal of Electroanalytical Chemistry 575 (2005) 61-74.

[19] K. Yasuda, K.Kondo, T.Nohira, R.Hagiwara, Journal of the Electrochemical Society 161-7 (2014) D3097-D3104.

[20] A. J. Bard, R. L. Faulkner, Electrochemistry: principles, methods and applications, Wiley Ed., New York, 1980.

[21] C. Nourry, L. Massot, P. Chamelot, P. Taxil, Electrochimica Acta 53 (2008) 2650–2655.

[22] P. Taxil, L. Massot, C. Nourry, M. Gibilaro, P. Chamelot, L. Cassayre, Journal of Fluorine Chemistry 130 (2009) 94-101.

[23] Binary Alloy Phase Diagrams, Second Edition ASM International (1996).

[24] W. Weppner, R.A. Huggins, Journal of the Electrochemical Society 124 (1977) 1569-77.

[25] W. Weppner, R.A. Huggins, Journal of the Electrochemical Society 125 (1978) 5-14.

[26] G. Picard, Y. Mottot, B. Trémillon Proceedings - Electrochemical Society 84 (1984) 585-90.

[27] P. Taxil, Journal of the Less Common Metals 113 (1985) 89-98.

[28] C. Nourry, L. Massot, P. Chamelot, P. Taxil, Journal of Applied Electrochemistry 39 (2009) 927-933.

Legend of Figures and Tables

Figure 1:

Cyclic voltammograms plotted on Mo electrode at 100 $mV.s^{-1}$ and 840°C for LiF-CaF_2-LaF_3 (0.138 $mol.kg^{-1}$) (grey line) and LiF-CaF_2-PrF_3 (0.136 $mol.kg^{-1}$) (black line) systems. Inset: variation of La(III) (grey squares and triangles) and Pr(III) (black discs and diamonds) reduction peak potential potentials and current densities versus the square root of the potential scan rate.

Figure 2:

Linear relationships between the cathodic peak current density and the concentration ($mol.kg^{-1}$) in LiF-CaF_2at 840 °C for La(III)/La (grey) and Pr(III)/Pr (black) systems

Figure 3:

Variation of the logarithm of the diffusion coefficient versus the inverse of the absolute temperature

Figure 4:

Extrapolation at infinite dilution of $E_{Ln(III)/Ln} - \frac{RT}{3F} ln([Ln(III)])$ versus [Ln(III)]

Figure 5:

Linear relationships between added normalized quantity of Li_2O and the remaining Ln(III) normalized content in the bath.

Figures 6a and 6b:

Superimposition of cyclic voltammograms plotted of reactive Ni, Cu and Fe electrodes at 100 $mV.s^{-1}$ and 840°C for $LiF-CaF_2-LaF_3$ (0.138 $mol.kg^{-1}$) (6a) and $LiF-CaF_2-PrF_3$ (0.136 $mol.kg^{-1}$) (6b) systems.

Figure 7

Open-circuit chronopotentiograms of the $LiF-CaF_2-LaF_3$ and $LiF-CaF_2-PrF_3$ systems on iron electrode at 840°C.

Figures 8a and 8b

Open-circuit chronopotentiograms of the $LiF-CaF_2-LaF_3$ (8a) and $LiF-CaF_2-PrF_3$ (8b) systems on copper electrode at 840°C.

Figures 9a and 9b

Open-circuit chronopotentiograms of the $LiF-CaF_2-LaF_3$ (9a) and $LiF-CaF_2-PrF_3$ (9b) systems on nickel electrode at 840°C.

Table 1:

Depolarization potential values of Ln-M alloys formation (Ln = La, Pr; M = Ni, Cu, Fe) at 840°C obtained by cyclic voltammetry at 100 $mV.s^{-1}$.

Table 2:

Gibbs energiy of Cu/Ln compounds (Ln = La, Pr).

Table 3:

Gibbs energy of Ni/Ln compounds (Ln = La, Pr).

Table 4:

Gibbs energy of Fe/Pr compounds.

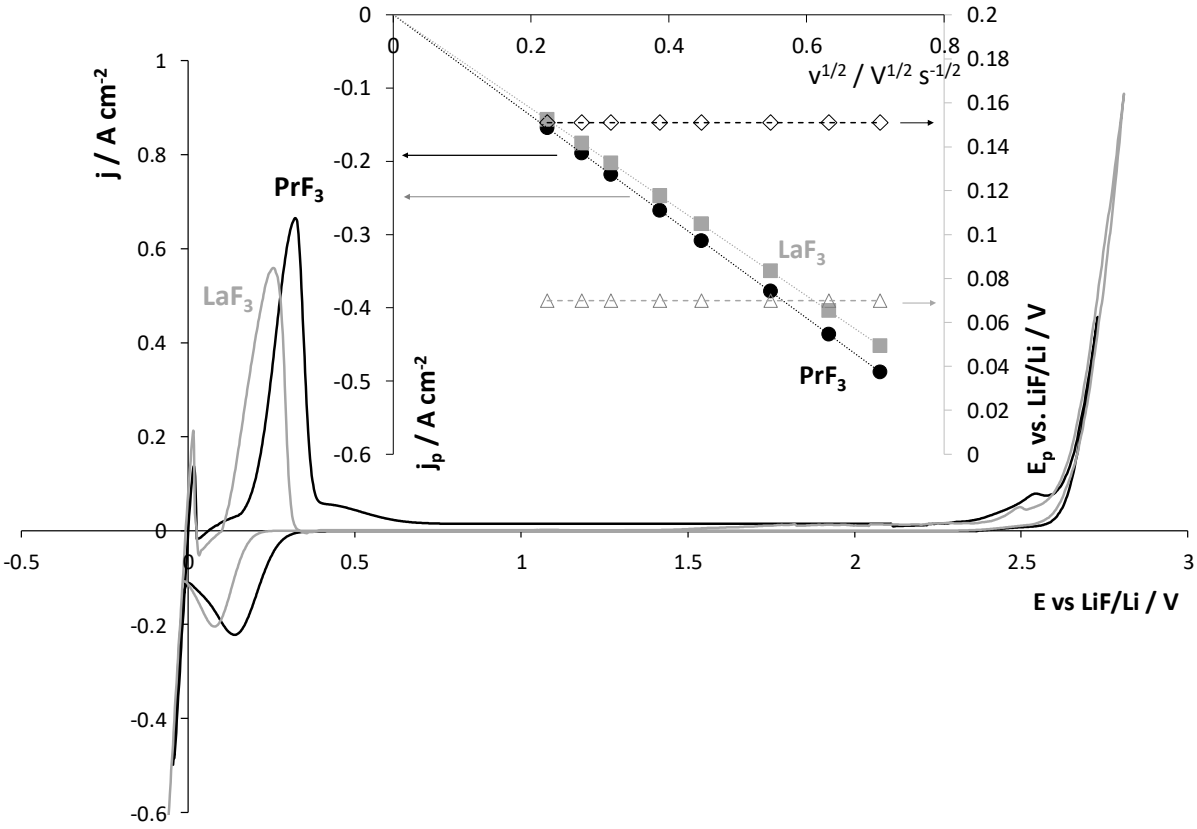
j / A cm-2
E vs LiF/Li / V
PrF3
LaF3
jp / A cm-2
v1/2 / V1/2 s-1/2
Ep vs. LiF/Li / V

Figure 1

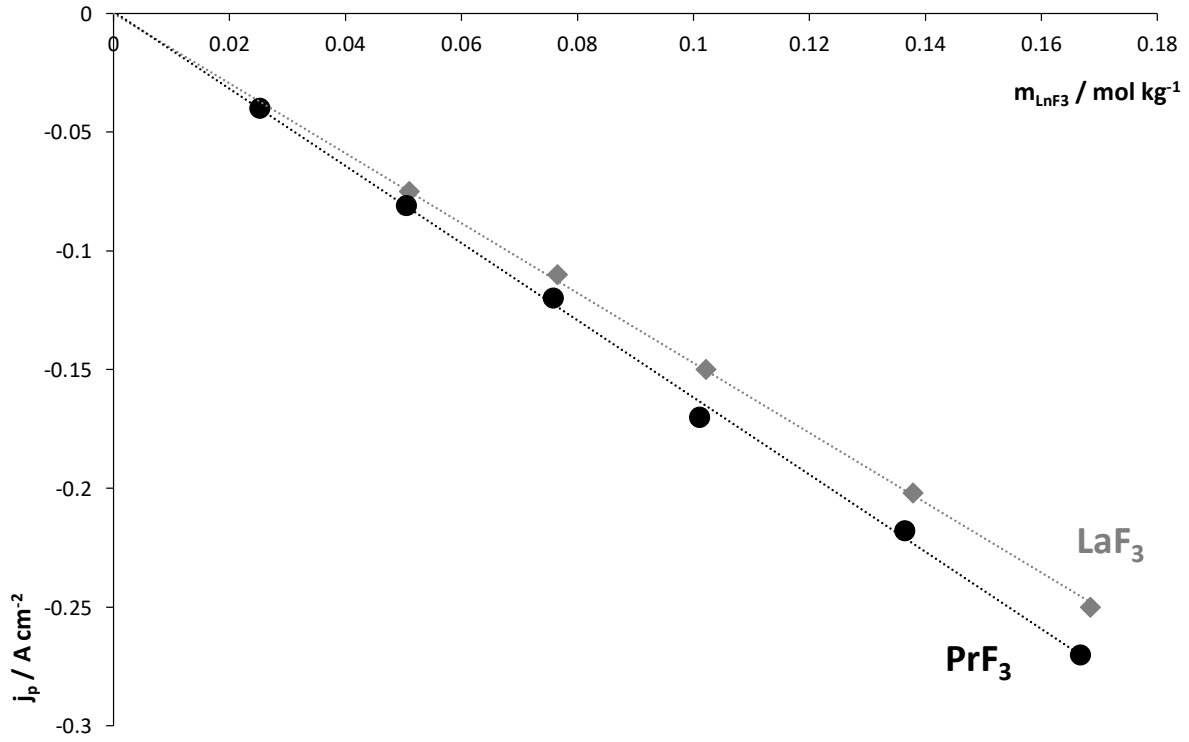
jp / A cm-2
mLnF3 / mol kg-1
LaF3
PrF3

Figure 2

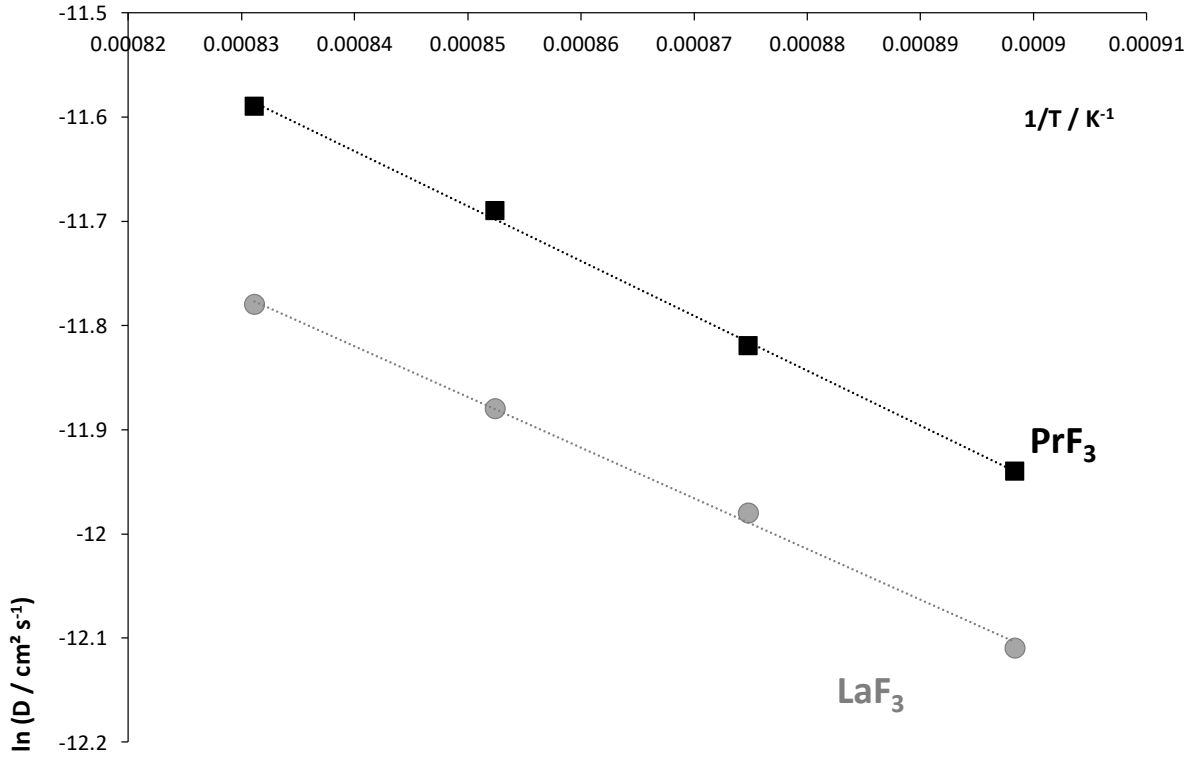

Figure 3

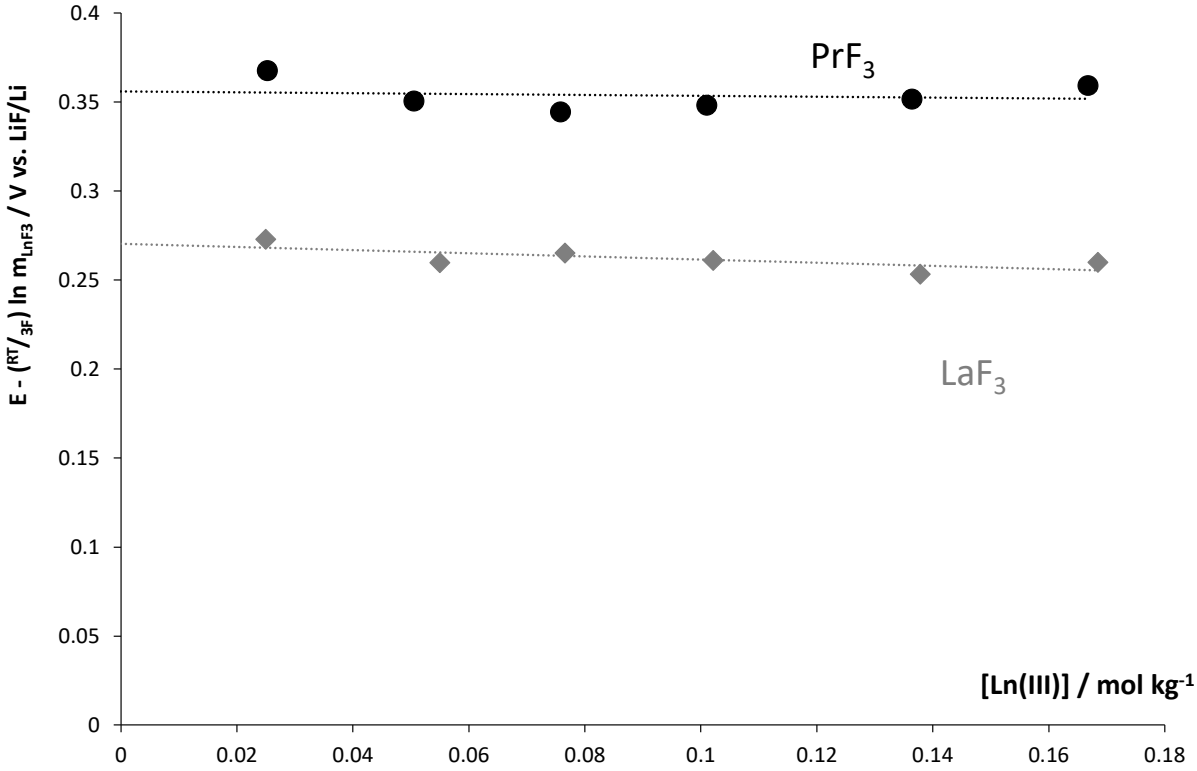

Figure 4

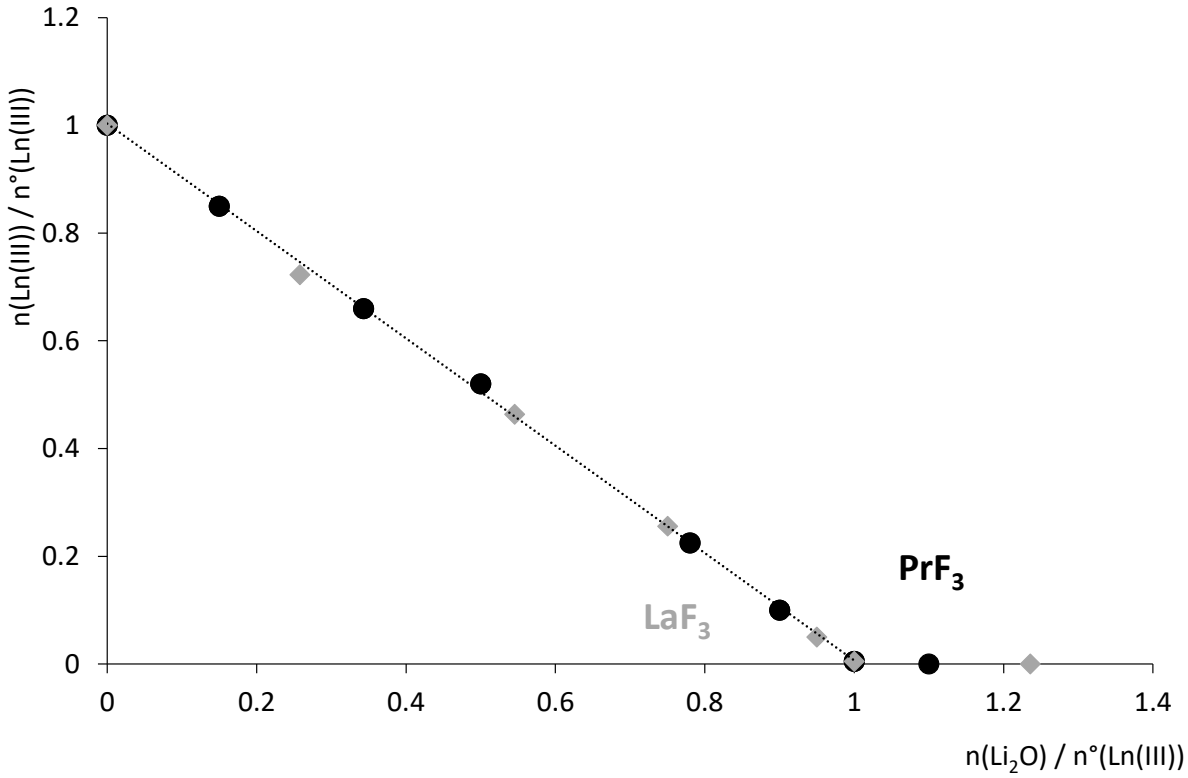

Figure 5

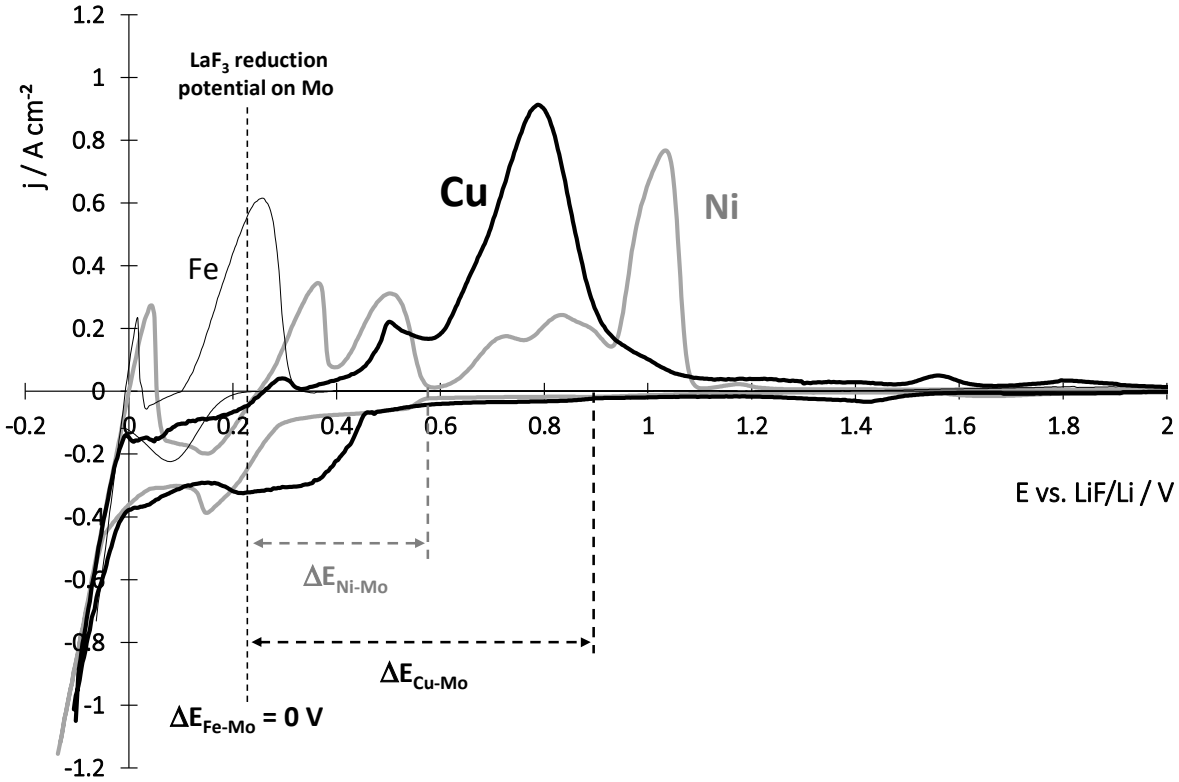

Figure 6a

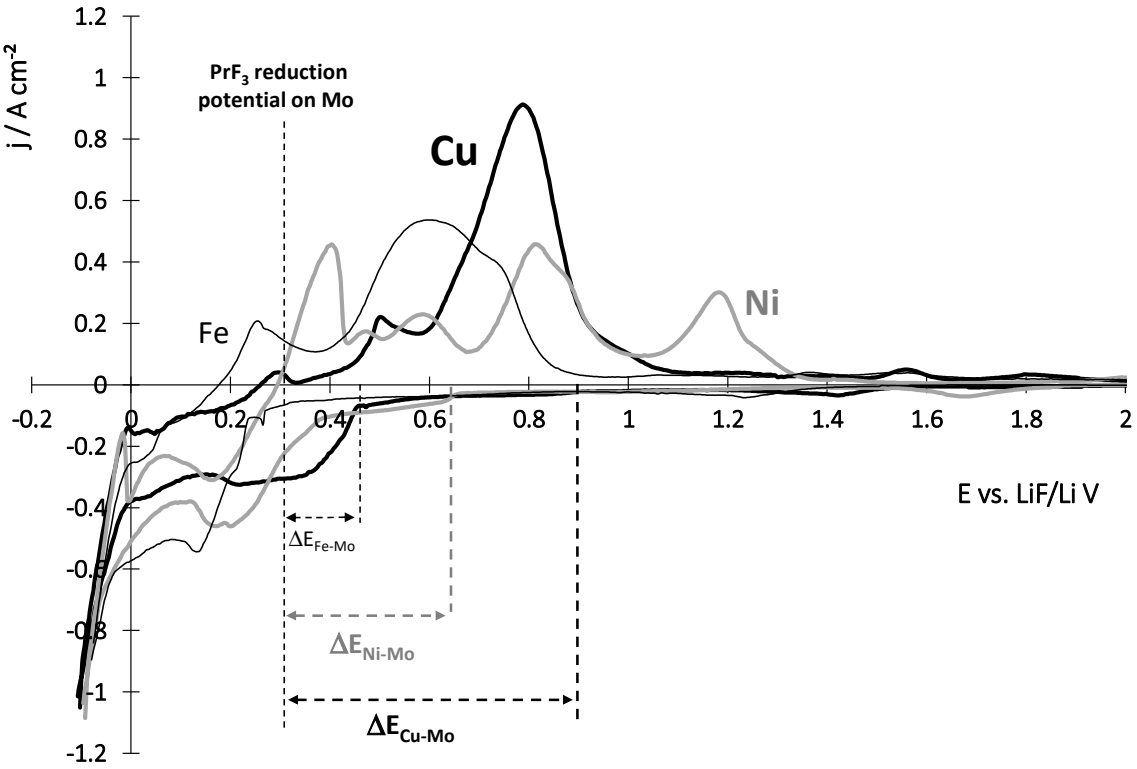

Figure 6b

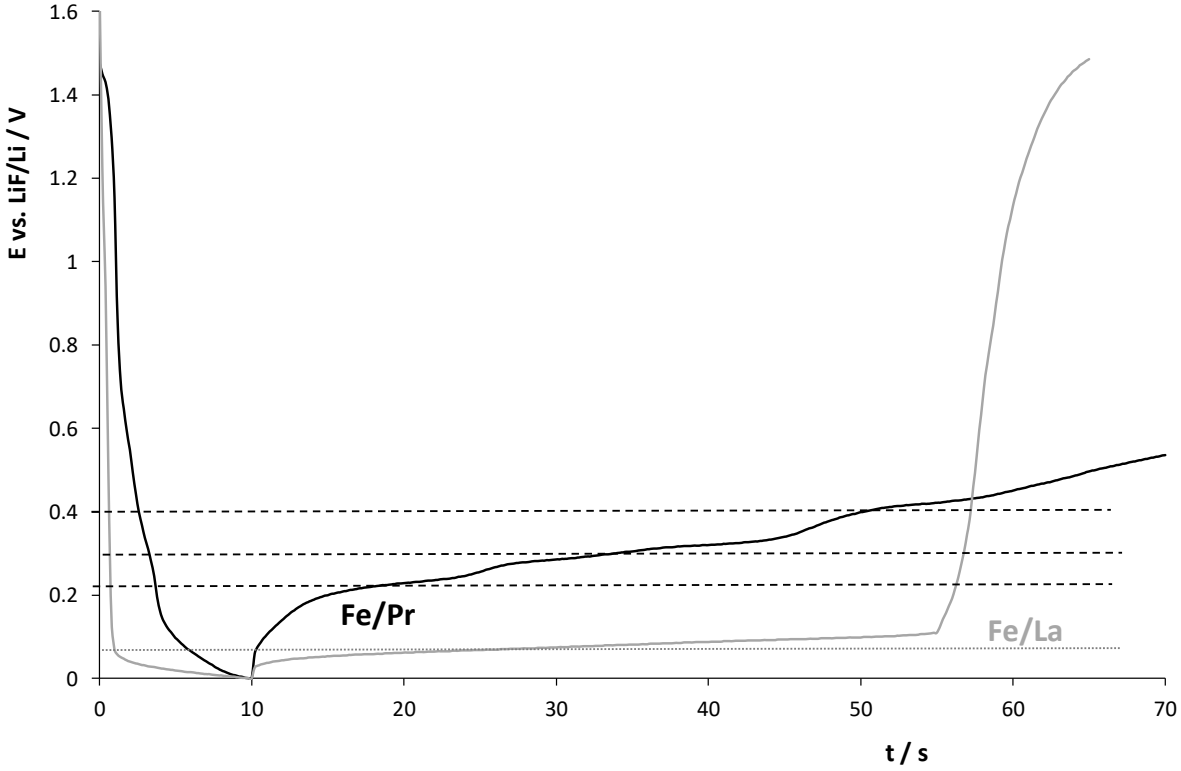

Figure 7

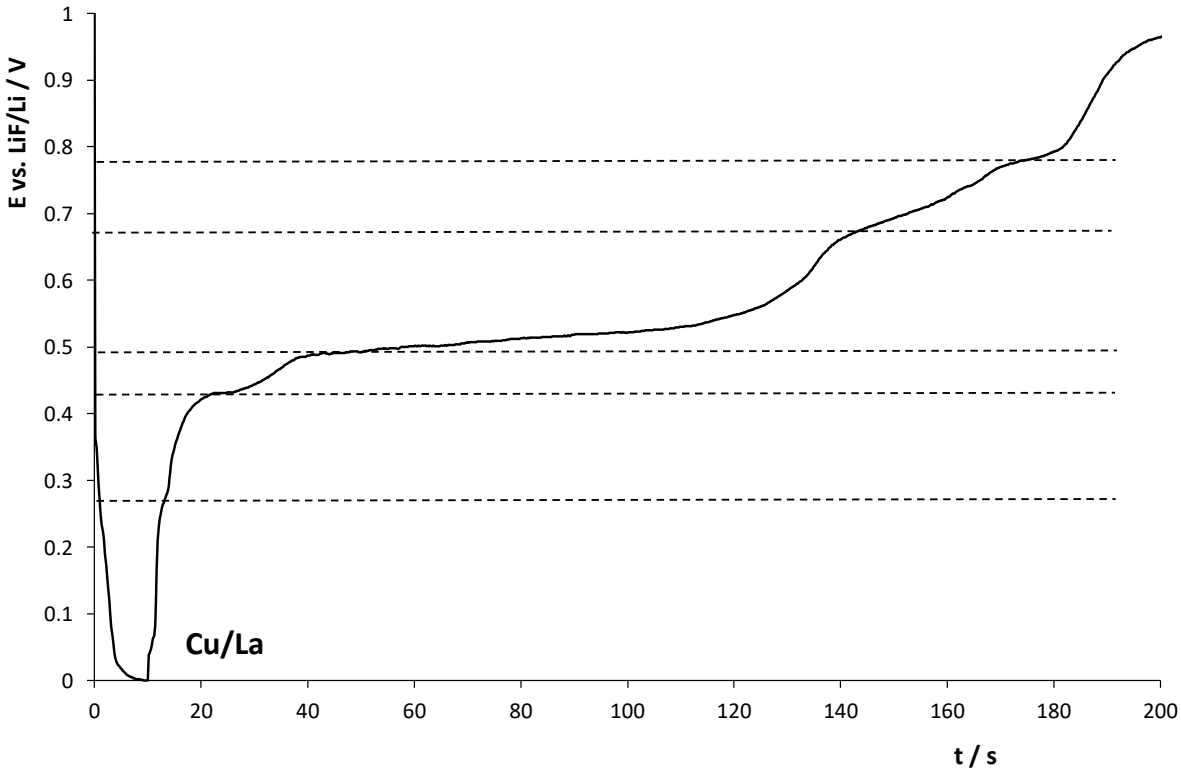

Figure 8a

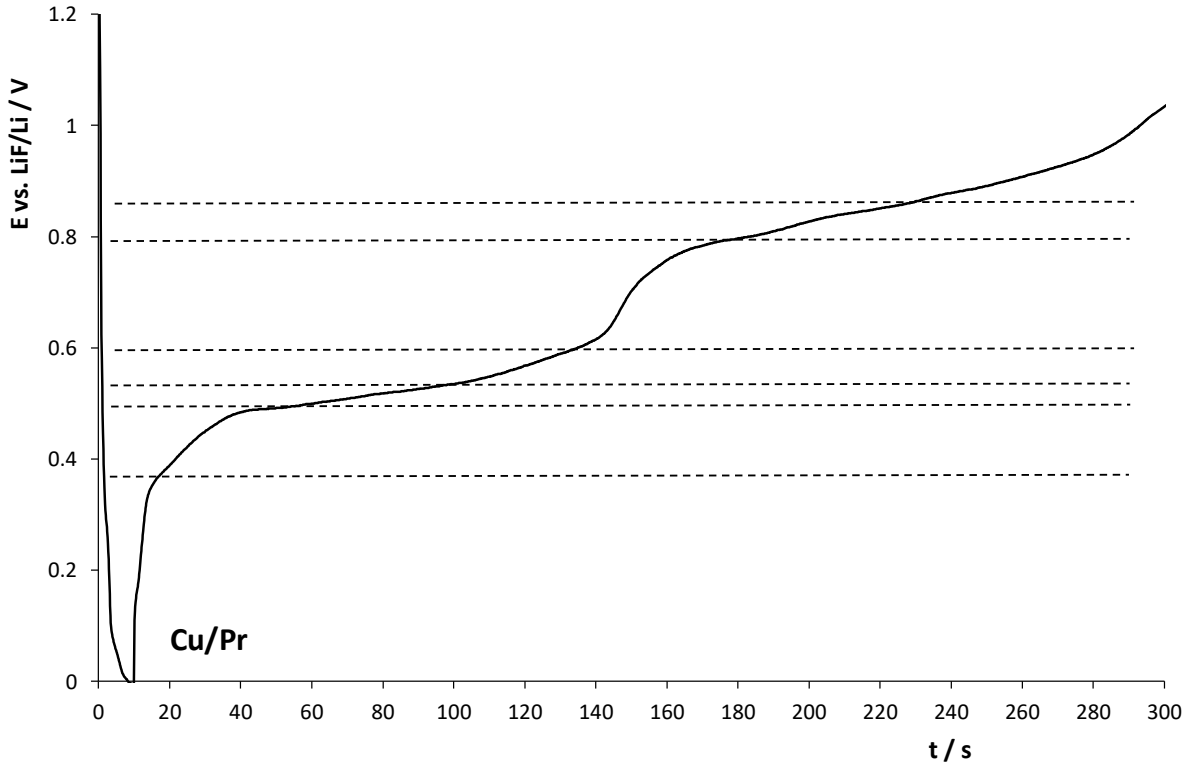

Figure 8b

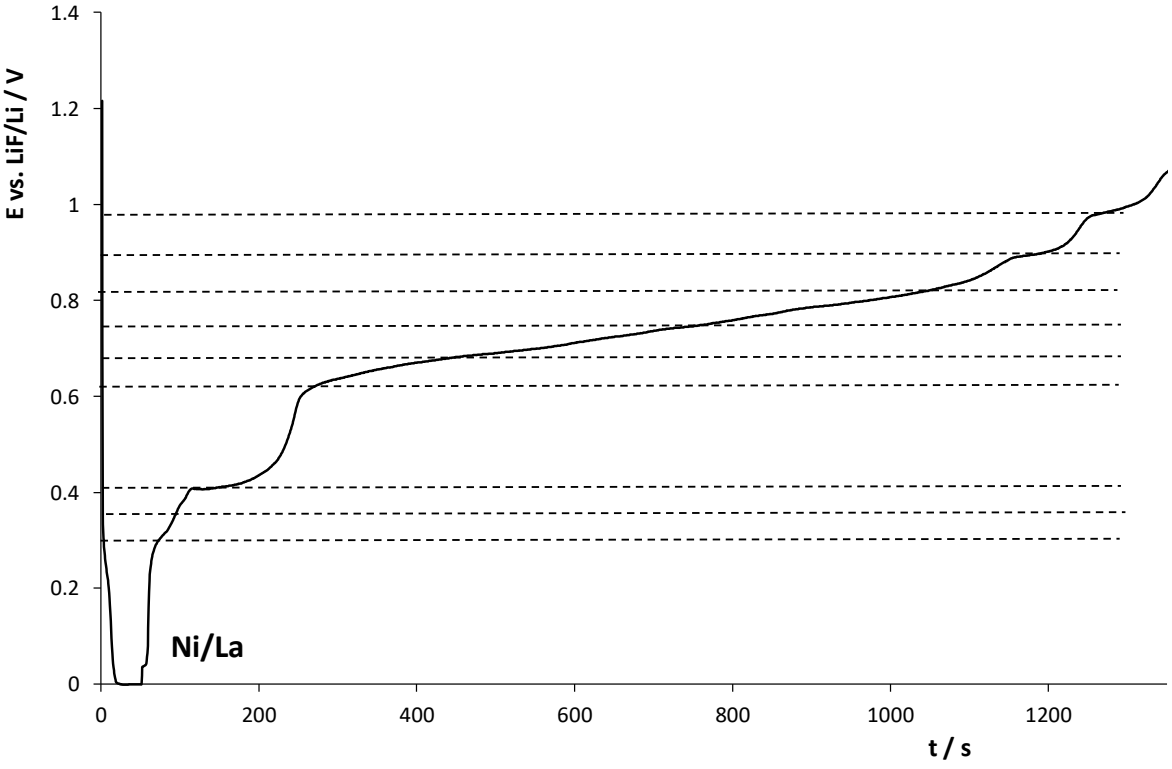

Figure 9a

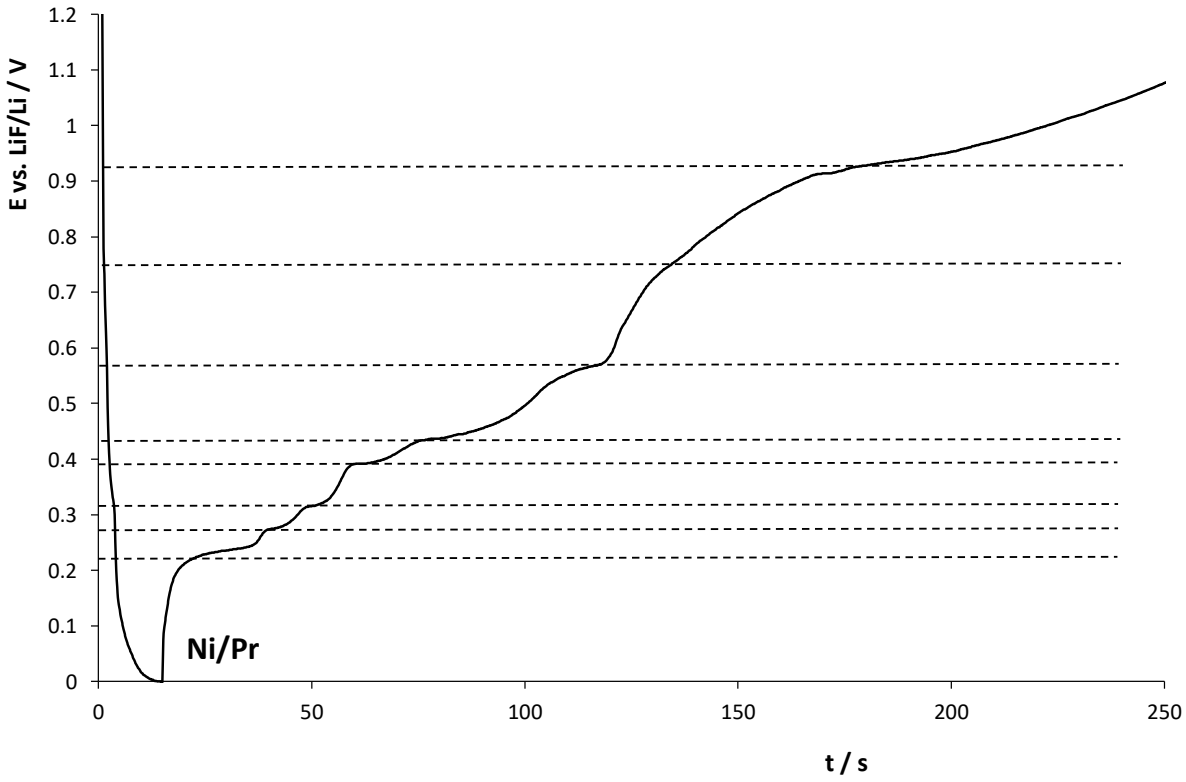

Figure 9b

Depolarisation (V)	Ni	Cu	Fe
La(III)/La	0.38	0.68	0
Pr(III)/Pr	0.35	0.6	0.17

Table 1

Cu/Ln compounds	$\Delta_f G°$ (kJ mol^{-1})			
	840°C	**870°C**	**900°C**	**930°C**
CuPr	-45.4	-11.0	-26.3	-31.8
Cu_2Pr	-101.6	-99.7	-92.6	-98.1
Cu_4Pr	-179.8	-185.7	-185.9	-204.9
Cu_5Pr	-310.3	-298.6	-296.4	-327.7
Cu_6Pr	-462.6	-468.4	-474.3	-501.4
CuLa	-45.2	-25.7	-41.7	-60.5
Cu_2La	-109.7	-97.0	-108.3	-140.4
Cu_5La	-222.9	-191.1	-192.8	-251.6
Cu_6La	-371.1	-322.2	-312.7	-416.6

Table 2

Ni/Ln compounds	$\Delta_f G°$ (kJ mol^{-1})			
	840°C	**870°C**	**900°C**	**930°C**
$NiPr_3$	-18.2	-13.0	-31.8	-32.0
Ni_3Pr_7	-35.9	-32.7	-72.3	-88.5
NiPr	-57.8	-41.7	-87.6	-116.0
Ni_2Pr	-123.2	-118.7	-227.4	-268.0
Ni_3Pr	-225.1	-214.2	-435.0	-474.4
Ni_7Pr_2	-376.5	-383.0	-669.2	-713.2
Ni_5Pr	-390.0	-389.8	-588.8	-617.2

$NiLa_3$	-20.2	-12.4	-14.7	-13.0
Ni_3La_7	-37.4	-28.8	-28.4	-31.8
NiLa	-96.8	-98.2	-87.7	-104.1
Ni_3La_2	-203.4	-213.7	-177.5	-216.7
Ni_2La	-226.4	-226.4	-210.9	-234.6
Ni_3La	-370.3	-399.0	-345.2	-371.5
Ni_7La_2	-542.3	-574.1	-528.8	-565.2
Ni_5La	-467.4	-495.8	-473.7	-507.0

Table 3

Fe/Ln compounds	**$\Delta_f G°$ (kJ mol^{-1})**			
	840°C	**870°C**	**900°C**	**930°C**
Fe_2Pr	-25.7	-21.1	-40.8	-42.5
$Fe_{17}Pr_2$	-81.1	-95.5	-140.7	-157.8

Table 4

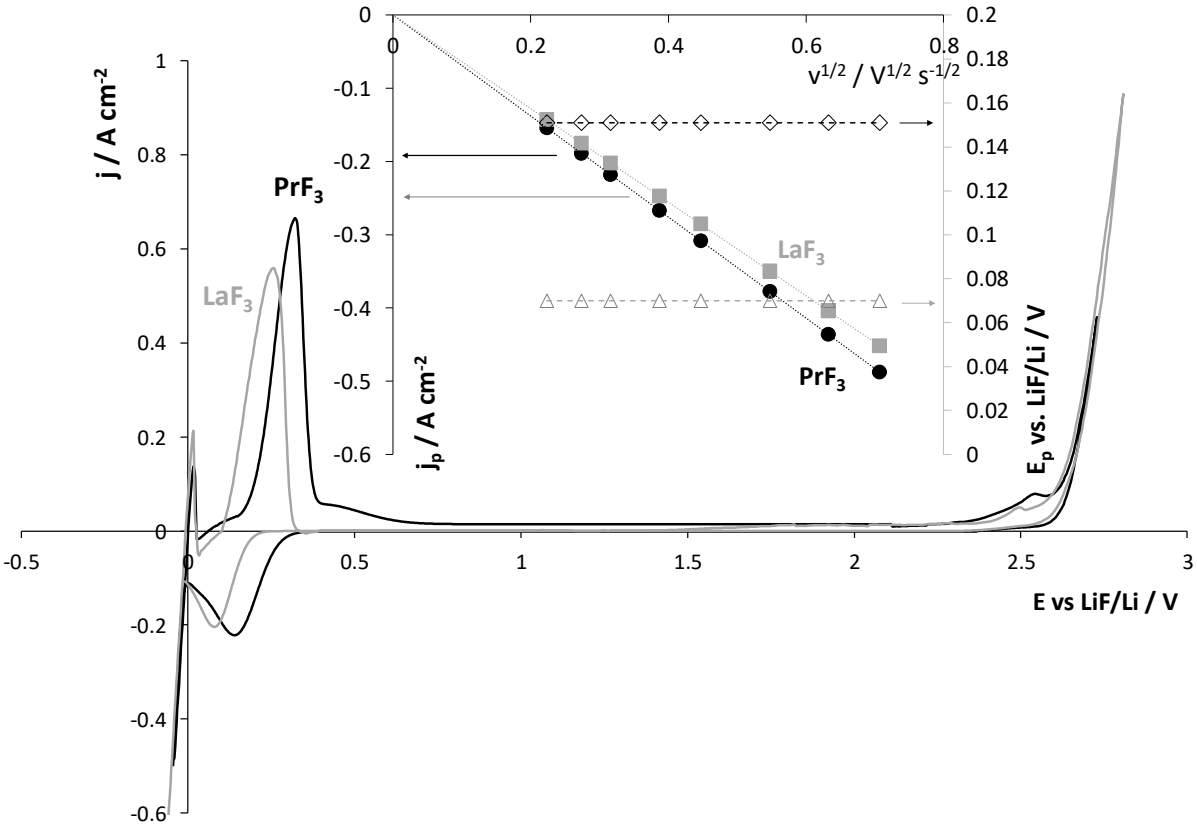

Figure 1

Cyclic voltammograms plotted on Mo electrode at 100 $mV.s^{-1}$ and 840°C for LiF-CaF_2-LaF_3 (0.138 $mol.kg^{-1}$) (grey line) and LiF-CaF_2-PrF_3 (0.136 $mol.kg^{-1}$) (black line) systems. Inset: variation of La(III) (grey squares and triangles) and Pr(III) (black discs and diamonds) reduction peak potential potentials and current densities versus the square root of the potential scan rate.